Journal of Quantitative Spectroscopy & Radiative Transfer 303 (2023) 108597

Contents lists available at ScienceDirect

Journal of Quantitative Spectroscopy & Radiative Transfer

journal homepage: www.elsevier.com/locate/jqsrt

Valence and Rydberg excitations of 2-fluorotoluene in the 4.4–10.8 eV photoabsorption energy region

P.A.S. Randi[a], S. Kumar[b,1], A.I. Lozano[b], M.H.F. Bettega[a], S.V. Hoffmann[c], N.C. Jones[c], A. Souza Barbosa[a,*], P. Limão-Vieira[a,b,*]

[a] Departamento de Física, Universidade Federal do Paraná, Caixa Postal 19044, Curitiba 81531-980, Paraná, Brazil
[b] Atomic and Molecular Collisions Laboratory, CEFITEC, Department of Physics, NOVA School of Science and Technology, Universidade NOVA de Lisboa, Caparica 2829-516, Portugal
[c] ISA, Department of Physics and Astronomy, Aarhus University, Ny Munkegade 120, Aarhus C DK-8000, Denmark

ARTICLE INFO

Article history:
Received 14 January 2023
Revised 29 March 2023
Accepted 29 March 2023
Available online 30 March 2023

Keywords:
2-fluorotoluene
C_7H_7F
electronic excitation
Vibrational excitation
Rydberg series
Ab initio calculations
Photoabsorption
Synchrotron radiation

ABSTRACT

The electronic state spectroscopy of 2-fluorotoluene in the gas phase has been investigated for the first time using high-resolution vacuum ultraviolet photoabsorption experiments in the 4.4–10.8 eV energy-range, with absolute cross-section measurements obtained. Additionally, we also present a novel set of ab initio calculations (vertical excitation energies and oscillator strengths) at two different levels of theory, equation-of-motion coupled-cluster singles and doubles (EOM-CCSD) and time-dependent density functional theory (TD-DFT). These are used in the assignment of valence, mix valence-Rydberg and Rydberg transitions, with the associated vibronic series analysed. The measured absolute photoabsorption cross-sections have been used to calculate the photolysis lifetime of 2-fluorotoluene in the Earth's atmosphere.

1. Introduction

Isomeric fluorotoluenes, *ortho*- (2-C_7H_7F), *meta*- (3-C_7H_7F) and *para*-fluorotoluene (4-C_7H_7F), have been extensively investigated either by experimental [1–15,15–20] or theoretical methods [4,11–15,17,19] (and references therein) due to relevant intramolecular dynamics governing internal rotation of the methyl group. The present work is the first of a set devoted to the electronic state spectroscopy of isomeric halotoluenes and the role of these trace gases in atmospheric chemistry and physics.

This is a continuation of a study in line with previous investigations of the electronic excitation of toluene [21] and difluorotoluenes [22] by high-resolution photoabsorption experiments and quantum chemical calculations. To our knowledge there are neither previous experimental measurements on electron energy loss (EEL) nor photoabsorption spectroscopies for 2-C_7H_7F in the energy range covered in the present work (4.4–10.8 eV). However, a literature survey reveals that Hammond et al. [23] and Cave and Thompson [24] have reported absorption spectra of *ortho*-fluorotoluene in the energy range 5.6–9.5 eV (220–130 nm) and 4.5–4.9 eV (275–250 nm), respectively, the latter suggesting the (0–0) transition of the lowest-lying band at 4.659 eV (37576 cm^{-1}). These studies included no assignments of the electronic transitions.

The ionisation energy to the ionic electronic ground-state has been determined through equilibrium constant measurements of Lias and Ausloss [25], while Palmer et al. [26] and Watanabe et al. [27] reported He(I) photoelectron spectra of the valence shell orbitals. Infrared spectra have been obtained to provide a consistent set of vibrational assignments [24,28–30], whilst fluorescence and emission spectra have been reported in the wavelength range 270–310 nm [31] (4.000–4.592 eV) and 250–310 nm [32] (4.000–4.959 eV). Yang *et al.* [1] reported photodissociation of 2-C_7H_7F at 193 nm (6.424 eV) with rotationally resolved emission of HF.

In this paper we report a comprehensive investigation of 2-C_7H_7F electronic state spectroscopy by combining experimental high-resolution vacuum ultraviolet (VUV) photoabsorption with calculations performed using theoretical *ab initio* methods of the

* Corresponding authors at: Departamento de Física, Universidade Federal do Paraná, Caixa Postal 19044, Curitiba 81531-980, Paraná, Brazil.
E-mail addresses: alessandra@fisica.ufpr.br (A.S. Barbosa), plimaovieira@fct.unl.pt (P. Limão-Vieira).
[1] Current address: Chemical Sciences Division, Lawrence Berkeley National Laboratory, One Cyclotron Road, Berkeley, 94720, California, USA

https://doi.org/10.1016/j.jqsrt.2023.108597

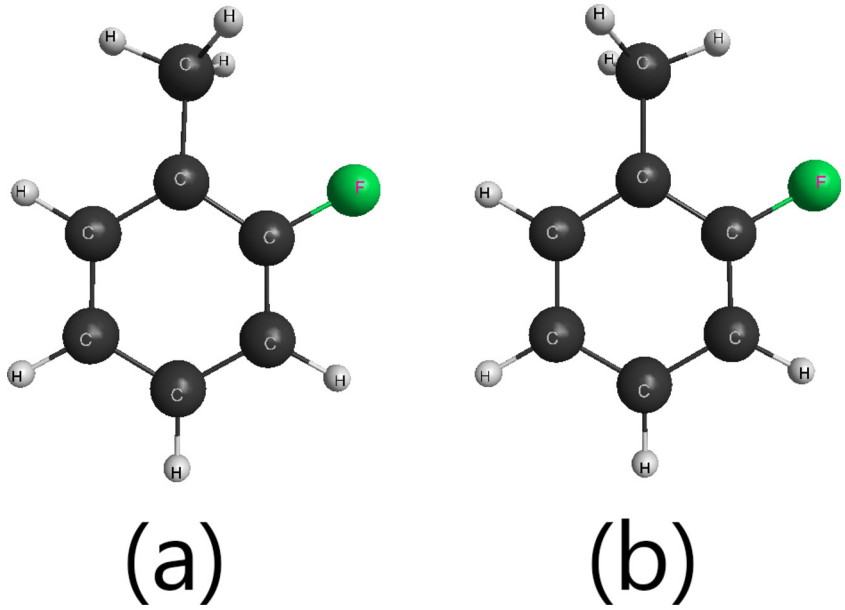

Fig. 1. Calculated structure of the two lowest-energy conformers of 2-fluorotoluene, 2-C_7H_7F optimised at DFT/CAMB3LYP/aug-cc-pVDZ level.

vertical excitation energies and oscillator strengths for the neutral electronic transitions. The fine structure observed across the entire photon energy range (10.8–4.4 eV, 114 < λ < 281 nm) is assigned here for the first time. In the next section we present the computational methods employed in the calculations. In Section 3 we provide a brief summary of the structure and properties of 2-fluorotoluene and in Section 4 we present a brief discussion of the experimental details. Section 5 is devoted to the results and discussion, and the absolute photoabsorption cross sections are used to calculate photolysis rates from 0–50 km altitude in the Earth's atmosphere. Finally, some conclusions that can be drawn from this study are given in Section 6.

2. Computational details

Assignment of 2-fluorotoluene absorption features has been performed with the aid of theoretical calculations on the electronic structure and properties of the electronically excited states. We have used two different levels of accuracy, equation-of-motion coupled-cluster singles and doubles (EOM-CCSD) [33–36] and time-dependent density functional theory (TD-DFT) [37,38], to obtain vertical excitation energies and oscillator strengths. The calculated spectrum at the EOM-CCSD/aug-cc-pVDZ level gives a better agreement with the experiment for the lowest-lying excited states up to ∼7 eV (Table S1), while TD-DFT/CAMB3LYP/aug-cc-pVDZ level of theory [39] is more attuned for higher excitation energies (Tables 1 and S2).

Geometry optimisation revealed two equilibrium conformations of C_s symmetry differing by a 60-degree rotation of the methyl group, as depicted in Fig. 1 (see also Fig. S1 for bond lengths and bond angles). From the DFT/CAMB3LYP/aug-cc-pVDZ calculation, performed with the GAMESS computational package [40], the second conformer ("b" in Fig. 1) is 0.027 eV above the first ("a" in Fig. 1). However, harmonic frequencies calculated with the same functional and basis set, show that an imaginary frequency for the second conformer is obtained, indicating therefore that this is actually a saddle point associated with an unstable configuration of the molecule. To support this finding, additional harmonic frequencies were calculated with B3LYP and PBE0 functionals (not shown here) and confirm the results. To further investigate the stability of these conformers a potential energy curve (PEC) along the rotation of the methyl group was calculated and is shown in Fig. S2. We observe three minima associated with the three possible stable equilibrium geometries of the first conformer (due to the three methyl H atoms), and three maxima associated with the unstable positions associated with the three possible configurations of the second conformer. It is worth noting that an identical behaviour was reported by Serralheiro et al. [21] for the toluene molecule.

The vertical excitation energies and properties of the electronically excited states were calculated in the optimized geometry of the ground-state of the stable conformer. The TD-DFT/CAMB3LYP/aug-cc-pVDZ and the EOM-CCSD/aug-cc-pVDZ calculations were performed with GAMESS [40] and Psi4 [41] computational packages, respectively.

3. Structure and properties of 2-fluorotoluene

The 2-fluorotoluene molecule has C_S symmetry (A′ and A″) in its electronic ground state and the calculated outermost valence electronic configuration of the $\tilde{X}\ ^1A'$ ground state, at the TD-DFT/aug-cc-pVDZ and EOM-CCSD/aug-cc-pVDZ levels are: ... $(16a')^2\ (17a')^2\ (18a')^2\ (1a'')^2\ (19a')^2\ (20a')^2\ (2a'')^2\ (21a')^2\ (22a')^2\ (23a')^2\ (3a'')^2\ (24a')^2\ (4a'')^2\ (5a'')^2$ and ... $(16a')^2\ (17a')^2\ (1a'')^2\ (18a')^2\ (19a')^2\ (20a')^2\ (21a')^2\ (2a'')^2\ (22a')^2\ (23a')^2\ (24a')^2\ (3a'')^2\ (4a'')^2\ (5a'')^2$, respectively. For a complete electronic configuration see the Supplementary Information (SI). The highest occupied molecular orbital (HOMO) 5a″ and the second highest occupied molecular orbital (HOMO-1) 4a″ have π character (Table S1), whereas at the TD-DFT/CAMB3LYP/aug-cc-pVDZ level the HOMO-2 (24a′), HOMO-4 (23a′) and HOMO-5 (22a′) have $\sigma_{CC}/\bar{n}_F$, σ_{CCC}, and $\sigma_{CC}/\bar{n}_F$ character, respectively (Table 1). The VUV photoabsorption features (Figs. 2 to 7) have been assigned to electronic excitations, due to the promotion of an electron from the highest occupied molecular orbitals to valence and Rydberg character orbitals (see Tables 1 and S1 for the calculated dominant excitation energies and oscillator strengths).

The fine structure discernible in the photoabsorption spectrum has been assigned to fundamental vibrational modes (Tables 2 to 4) based on the energies (and wavenumbers) calculated at the DFT/CAMB3LYP/aug-cc-pVDZ level of theory compared with the available experimental data [29,30] (see Tables S3 and S4). The Rydberg states have been assigned through knowledge of the ioni-

Table 1
Calculated vertical excitation energies (TD-DFT/CAMB3LYP/aug-cc-pVDZ level) (eV) and oscillator strengths (singlet states) of the main electronic states of 2-fluorotoluene, 2-C_7H_7F compared with experimental data and other work (energies in eV) (details in text).

State	E (eV)	f_L	HOMO	HOMO-1	Other	Exp. (eV)	Cross section (Mb)	Ref. [24]
			π (5a″)	π (4a″)				
$\tilde{X}$ ^{1}A′	–	–						
2 ^{1}A′	5.274	0.010894	π^*(6a″) (60%)	π^*(7a″) (32%)		4.647	4.22	4.659
3 ^{1}A′	5.975	0.008171	π^*(7a″) (50%)	π^*(6a″) (43%)		6.129	24.68	–
1 ^{1}A"	6.265	0.007254	3p/π^*(25a′) (89%)					
4 ^{1}A′	6.780	0.492196	π^*(7a″) (41%)	π^*(6a″) (49%)		6.858	212.39	–
5 ^{1}A′	6.861	0.685860	π^*(6a″) (31%)	π^*(7a″) (59%)				
7 ^{1}A′	8.144	0.022748	5p(8a″) (11%) + 4p′(9a″) (83%)			8.064	20.18	–
28 ^{1}A"	9.475	0.023819	9d(36a′) (12%)	6p/7s(35a′) (38%)	π^*(6a″) ← $\sigma_{CC}/\bar{n}_F$(22a′) (15%)	9.083	24.17	–
18 ^{1}A′	9.685	0.035695	π^*(12a″) (14%)	π^*(11a″) (47%)	3p(27a′) ← $\sigma_{CC}/\bar{n}_F$(24a′) (25%)	9.454	39.18	–
21 ^{1}A′	9.850	0.035532	π^*(13a″) (26%)		3p(26a′) ← σ_{CCC}(23a′) (35%)			
25 ^{1}A′	10.300	0.042230			3d(29a′) ← $\sigma_{CC}/\bar{n}_F$(24a′) (58%)	10.039	51.12	–

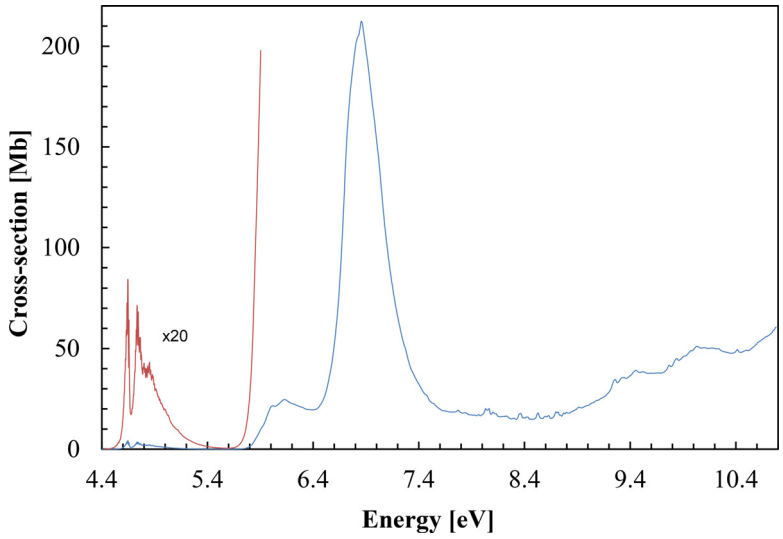

Fig. 2. The high resolution VUV photoabsorption spectrum of 2-fluorotoluene, 2-C_7H_7F in the 4.4–10.8 eV photon energy range.

sation states energies and the application of quantum defect theory (Table 5). The five lowest ionisation energies (IEs), which are needed to calculate the quantum defects associated with transitions to Rydberg orbitals (see Section 5.2), have been obtained experimentally at $(IE_1)_{ad}$ = 8.915 eV $(5a'')^{-1}$ [27], $(IE_2)_v$ = 9.53 eV $(4a'')^{-1}$ [26], $(IE_3)_v$ = 12.08 eV $(24a')^{-1}$ [26], $(IE_4)_v$ = 12.65 eV $(23a')^{-1}$ [26], and $(IE_5)_v$ = 14.00 eV $(3a'')^{-1}$ [26].

4. Experimental details

4.1. 2-fluorotoluene sample

The liquid sample used in the VUV measurements was purchased from Sigma-Aldrich, with a stated purity of ≥ 99%. The sample was degassed by repeated freeze–pump–thaw cycles.

4.2. VUV photoabsorption

The high-resolution vacuum ultraviolet (VUV) photoabsorption spectrum of 2-fluorotoluene was recorded using the AU-UV beam line of the ASTRID2 synchrotron facility at Aarhus University, Denmark (Fig. 2). The experimental apparatus has been described in detail elsewhere [42,43] so only a short review will be given here. Briefly, synchrotron radiation passes through a static gas sample and a photomultiplier is used to measure the transmitted light intensity. The incident wavelength is selected using a toroidal dispersion grating with 2000 lines/mm providing a resolution better than 0.075 nm, corresponding to 3 meV at the midpoint of the energy range studied. The sample pressure is measured using a capacitance manometer (Chell CDG100D). To ensure that the data is free of any saturation effects the absorption cross-sections were measured over the pressure range 0.02–1.31 mbar, with typical attenuations of less than 50%. The synchrotron beam current was monitored throughout the collection of each spectrum and background scans were recorded with the cell evacuated. Absolute photoabsorption cross sections are then obtained using the Beer-Lambert attenuation law: $I_t = I_0 \exp(-N\sigma l)$, where I_t is the radiation intensity transmitted through the gas sample, I_0 is that through the evacuated cell, N the molecular number density of the sample gas, σ the absolute photoabsorption cross section, and l the absorption path length (15.5 cm). Accurate cross-section values are obtained by recording the different absorption spectra in 5 or 10 nm sections, allowing an overlap of at least 10 points between the adjoining sections. In order to compensate for the constant beam decay in the storage ring, ASTRID2 operates in a “top-up” mode allowing the light intensity to be kept quasi-constant. The variations (∼2–3%) of the incident flux are therefore normalized to the beam current in the storage ring. The accuracy of the cross section is estimated to be better than ± 5%. Only when absorption by the sample is very weak ($I_0 \approx I_t$), does the error increase as a percentage of the measured cross section.

5. Results and discussion

The absolute high-resolution VUV photoabsorption cross-section of 2-fluorotoluene is shown in Fig. 2, extending from 4.4 to

Table 2
Proposed vibrational assignments in the 4.4–5.0 eV absorption band of 2-fluorotoluene, 2-C_7H_7F. ΔE values in meV.

Assignment	Energy (eV)	ΔE (ν'_{19})	ΔE (ν'_{20})	ΔE (ν'_{21})	ΔE (ν'_{22})	ΔE (ν'_{24})	ΔE (ν'_{25})	Ref. [16] (eV)
$p_1 21_1^0$	4.49(9)(s,w)	–	–	–	–	–	–	–
$p_2 21_1^0$	4.50(7)(s,w)	–	–	–	–	–	–	–
$p_5 21_0^1/19_1^0$	4.52(2)(s,w)	–	–	–	–	–	–	–
$p_6 21_1^0$	4.53(2)(s,w)	–	–	–	–	–	–	–
$p_7 21_1^0/22_1^0$	4.54(0)(s,w)	–	–	–	–	–	–	–
$p_8 21_1^0$	4.54(7)(s)	–	–	–	–	–	–	–
21_1^0	4.557	–	–	–	–	–	–	–
?	4.56(7)(s,w)	–	–	–	–	–	–	–
$p_1 21_0^0/25_1^0$	4.59(3)(s,w)	–	–	0.0 (−54)	–	–	–	–
$p_2 21_0^0/24_1^0$	4.60(0)(s,w)	–	–	0.0 (−47)	–	–	–	–
$p_3 21_0^0$	4.60(5)(s)	–	–	0.0 (−42)	–	–	–	–
$p_4 21_0^0$	4.613	–	–	0.0 (−34)	–	–	–	–
$p_5 21_0^0$	4.61(9)(s)	–	–	0.0 (−28)	–	–	–	–
$p_6 21_0^0$	4.62(5)(b)	–	–	0.0 (−22)	–	–	–	–
$p_7 21_0^0$	4.632	–	–	0.0 (−15)	–	–	–	–
$p_8 21_0^0$	4.638	–	–	0.0 (−9)	–	–	–	–
0_0^0	**4.647**	**–**	–	**0.0**	**–**	–	–	–
$p_9 21_0^0$	4.658	–	–	0.0 (+11)	–	–	–	–
$p_1 21_0^1$	4.68(4)(w)	–	–	91	–	–	–	–
$p_2 21_0^1$	4.68(9)(w)	–	–	89	–	–	–	–
$p_3 21_0^1/24_0^1$	4.69(4)(s,w)	–	–	89	–	47	–	4.696
$p_4 21_0^1/25_0^1$	4.703	–	–	90	–	–	56	4.706
$p_5 21_0^1/25_0^1$	4.70(9)(s)	–	–	90	–	–	62	4.706
$p_6 21_0^1$	4.715	–	–	90	–	–	–	–
$p_7 21_0^1$	4.720	–	–	88	–	–	–	–
21_0^1	4.735	–	–	88	–	–	–	–
$p_9 21_0^1/22_0^1$	4.745	–	–	87	98	–	–	4.745
$p_1 21_0^2/19_0^1$	4.772	125	–	88	–	–	–	4.772
$p_2 21_0^2/20_0^1$	4.775	–	128	86	–	–	–	4.775
$p_3 21_0^2$	4.783	–	–	89	–	–	–	–
$p_5 21_0^2$	4.791	–	–	82	–	–	–	–
$p_6 21_0^2$	4.799	–	–	84	–	–	–	–
$p_7 21_0^2$	4.80(4)(w)	–	–	84	–	–	–	–
21_0^2	4.822	–	–	87	–	–	–	–
$p_9 21_0^2$	4.833	–	–	88	–	–	–	–
22_0^2	4.840	–	–	–	95	–	–	–
$p_1 21_0^3$	4.860	–	–	88	–	–	–	–
$p_2 21_0^3$	4.863	–	–	88	–	–	–	–
$p_3 21_0^3$	4.871	–	–	88	–	–	–	–
$p_5 21_0^3$	4.878	–	–	87	–	–	–	–
$p_6 21_0^3$	4.885	–	–	86	–	–	–	–
$p_7 21_0^3$	4.88(8)(s)	–	–	84	–	–	–	–
21_0^3	4.912	–	–	90	–	–	–	–
$p_9 21_0^3$	4.91(7)(s)	–	–	84	–	–	–	–
$p_5 21_0^4$	4.96(3)(b)	–	–	85	–	–	–	–
21_0^4	4.999	–	–	87	–	–	–	–

(s) shoulder structure; (w) weak structure; (b) broad structure; (?) unassigned feature (the last decimal of the energy value is given in brackets for these less-resolved features).

10.8 eV and Figs. 3–7 show expanded views in the photon energy region. The major absorption bands can be classified as valence transitions of ($\pi^* \leftarrow \pi$) character and Rydberg series converging to the different ionisation energies. Tables 1 and S1 show the calculated vertical excitation energies and oscillator strengths at the TD-DFT/CAMB3LYP/aug-cc-pVDZ and EOM-CCSD/aug-cc-pVDZ levels, respectively, and compare with the experimental results. However, a close comparison between both sets of calculations shows that EOM-CCSD gives a better agreement with experiment up to ∼ 7eV, while TD-DFT/CAMB3LYP agrees reasonably well with the photoabsorption data above 7 eV. Therefore, the calculated data in Table S1 is shown up to 7.4 eV while Table 1 contains information on the vertical excitation energies up to 10.3 eV.

5.1. Valence state spectroscopy of 2-fluorotoluene

Many of the calculated electronically excited states show a mixed character where more than one transition has a significant character. Thus, the description hereafter relates to particle 1 ← hole 1 + particle 2 ← hole 2 (excited state ← ground state), where each hole-particle pair is associated with a distinct transition. On the basis of the EOM-CCSD calculations summarised in Table S1, the absorption bands centred at 4.647, 6.129 and 6.858 eV have been assigned to valence $\pi^*(7a'') \leftarrow \pi(5a'') + \pi^*(8a'') \leftarrow \pi(4a'')(2^1A' \leftarrow \tilde{X}^1A')$, $\pi^*(8a'') \leftarrow \pi(5a'') + \pi^*(7a'') \leftarrow \pi(4a'')(3^1A' \leftarrow \tilde{X}^1A')$ and $\pi^*(7a'') \leftarrow \pi(4a'') + \pi^*(8a'') \leftarrow \pi(5a'')(4^1A' \leftarrow \tilde{X}^1A')$ transitions, respectively, however features at 6.129 and 6.858 eV may also have a Rydberg character (see Section 5.2) and are assigned to $3s(25a') \leftarrow \pi(5a'')(1^1A'' \leftarrow \tilde{X}^1A')$ and $4p(6a'') \leftarrow \pi(4a'')(4^1A'' \leftarrow \tilde{X}^1A')$. With calculations using TD-DFT/CAMB3LYP (Table 2), these features have been assigned to $\pi^*(6a'') \leftarrow \pi(5a'') + \pi^*(7a'') \leftarrow \pi(4a'')(2^1A' \leftarrow \tilde{X}^1A')$, $\pi^*(7a'') \leftarrow \pi(5a'') + \pi^*(6a'') \leftarrow \pi(4a'')(3^1A' \leftarrow \tilde{X}^1A')$ and $\pi^*(6a'') \leftarrow \pi(4a'') + \pi^*(7a'') \leftarrow \pi(5a'')(4^1A' \leftarrow \tilde{X}^1A')$ transitions, although a mixed valence-Rydberg $3p/\pi^*(25a') \leftarrow \pi(5a'')(1^1A'' \leftarrow \tilde{X}^1A')$ character at 6.129 eV is also noted (see Section 5.2). Note that the feature at 6.858 eV can additionally be assigned to the $\pi^*(7a'') \leftarrow \pi(4a'') + \pi^*(6a'') \leftarrow \pi(5a'')(5^1A' \leftarrow \tilde{X}^1A')$ transition given its oscillator strength (Table 2).

The calculated transition energy for the lowest-lying excited state at EOM-CCSD level is overestimated by ∼0.4 eV when compared to the experimental value, whereas at the TD-DFT/CAMB3LYP level it is by 0.6 eV. The first band was also

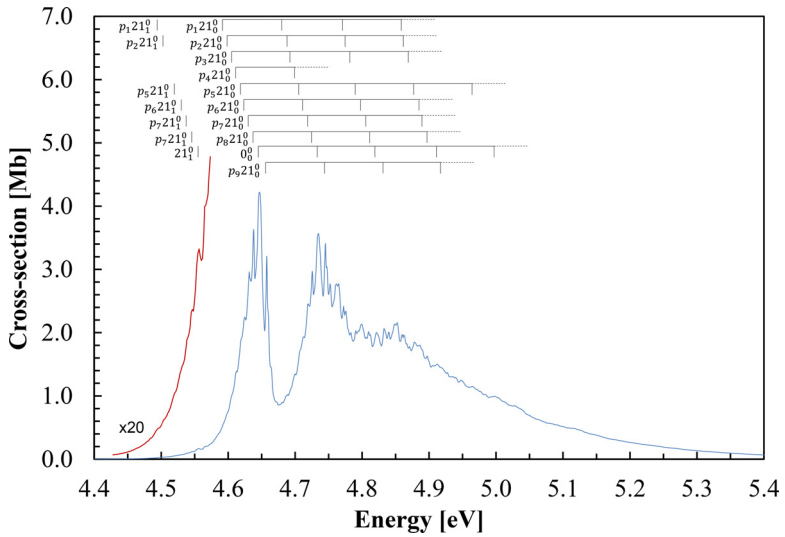

Fig. 3. The VUV photoabsorption spectrum of 2-fluorotoluene, 2-C_7H_7F in the 4.4–5.5 eV photon energy range. See text for details on the assignments.

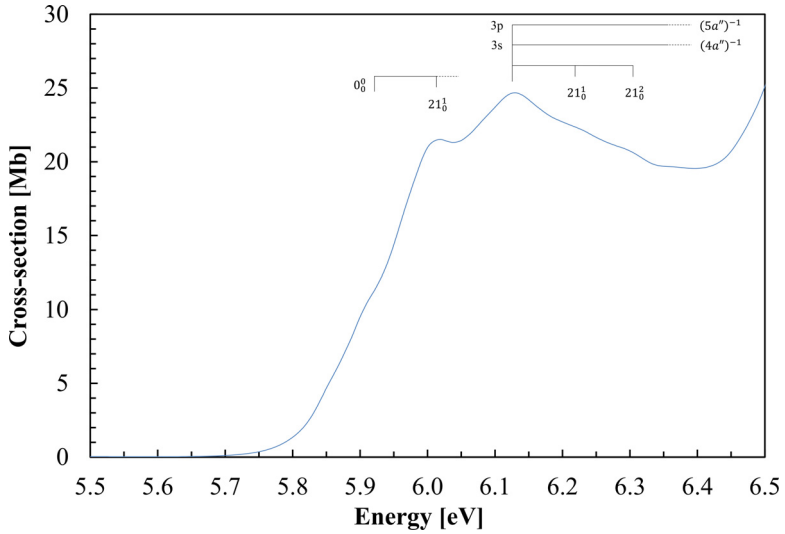

Fig. 4. VUV photoabsorption spectrum of 2-fluorotoluene, 2-C_7H_7F in the 5.5–6.5 eV photon energy range.

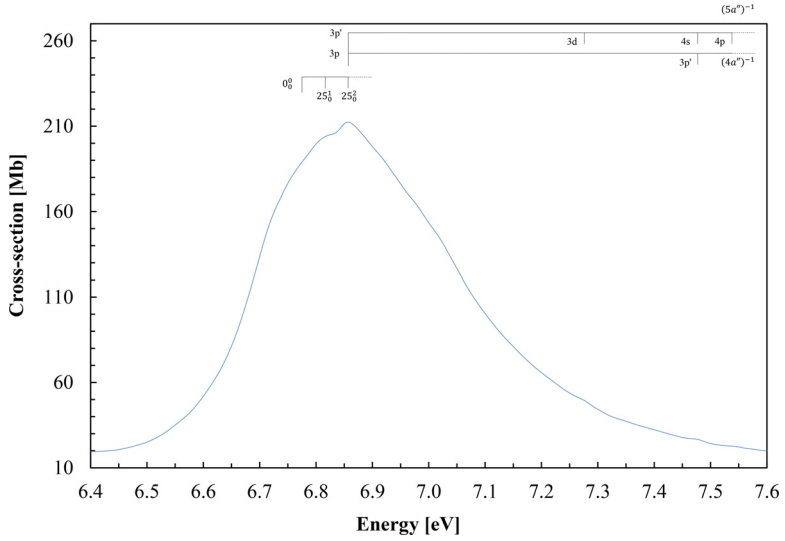

Fig. 5. VUV photoabsorption spectrum of 2-fluorotoluene, 2-C_7H_7F in the 6.4–7.6 eV photon energy range.

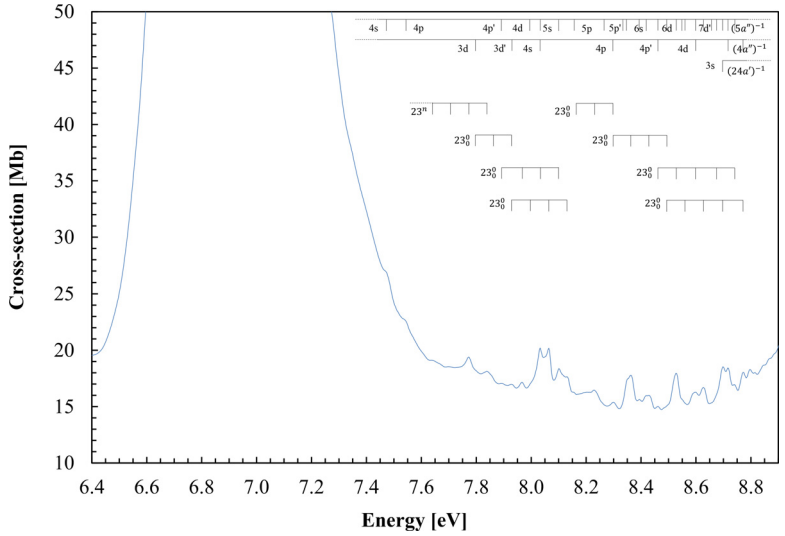

Fig. 6. VUV photoabsorption spectrum of 2-fluorotoluene, 2-C_7H_7F in the 6.4–8.9 eV photon energy range.

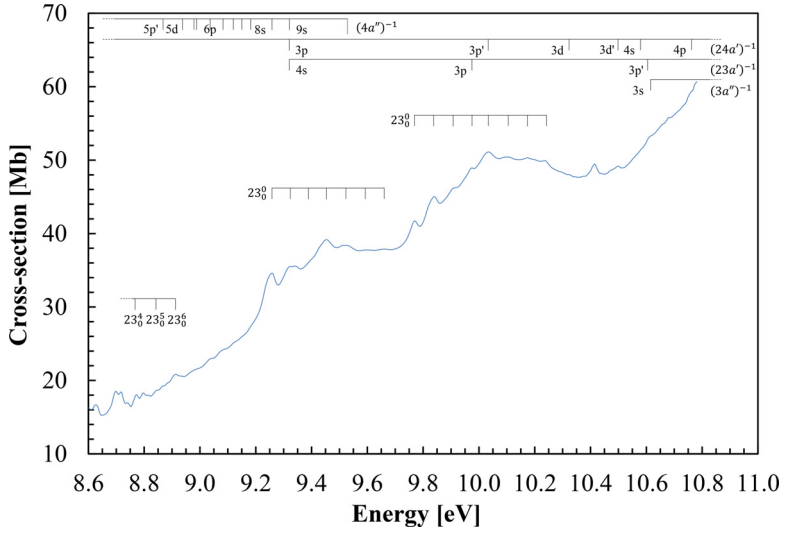

Fig. 7. VUV photoabsorption spectrum of 2-fluorotoluene, 2-C_7H_7F in the 8.6–10.8 eV photon energy range.

reported by Hammond et al. [23] at 4.659 eV and here with a maximum absolute cross-section of 4.22 Mb, whereas the second band peaks at 24.68 Mb and the third at 212.39 Mb (Tables 1 and S1). Finally, the VUV spectrum reveals other bands at 8.064, 9.083, 9.454 and 10.039 eV which are also assigned to valence, Rydberg and mixed valence-Rydberg transitions (Table 1). These have been assigned to $5p(8a'') + 4p'(9a'') \leftarrow \pi(5a'')(7^1A' \leftarrow \tilde{X}^1A')$, $9d(36a') \leftarrow \pi(5a'') + 6p/7s(35a') \leftarrow \pi(4a'') + \pi^*(6a'') \leftarrow \sigma_{CC}/\bar{n}_F(22a')(28^1A'' \leftarrow \tilde{X}^1A')$, $\pi^*(11a'') \leftarrow \pi(4a'') + \pi^*(12a'') \leftarrow \pi(5a'') + 3p(27a') \leftarrow \sigma_{CC}/\bar{n}_F(24a')(18^1A' \leftarrow \tilde{X}^1A')/\pi^*(13a'') \leftarrow \pi(5a'') + 3p(26a') \leftarrow \sigma_{CCC}(23a')(21^1A' \leftarrow \tilde{X}^1A')$ and $3d(29a') \leftarrow \sigma_{CC}/\bar{n}_F(24a')(25^1A' \leftarrow \tilde{X}^1A')$, with maximum cross-sections of 20.18, 24.17, 39.18 and 51.12 Mb, respectively. Note that most of the various spectral features overlap with many different Rydberg electronic states and the superposition of several vibrational modes. These contribute therefore to the broadening of the absorption features as well as to enhance others which by their nature would not manifest as intensely as they appear.

5.1.1. Valence and vibronic excitation in the range 4.4–5.4 eV

The 0_0^0 origin band of the lowest-lying excited state which also coincides with its vertical value is at 4.647 eV, with a cross-section of 4.22 Mb, and is in good agreement with the value of 4.652 eV (266.5 nm) [32] and 4.657 eV (37562 cm^{-1}) [16,31] from fluorescence spectroscopy measurements. It has been assigned in Table 1 to the promotion of an electron from the HOMO to LUMO+7 and from the HOMO-1 to the LUMO+9 to $\pi^*(7a'') \leftarrow \pi(5a'') + \pi^*(8a'') \leftarrow \pi(4a'')(2^1A' \leftarrow \tilde{X}^1A')$, and shows a large number of progressions that are detailed in Table 2. Analysis of this absorption region indicates that 9 progressions of the $\nu'_{21}(a')$ vibrational mode (C–F/C–H stretching, see Table S3) are dominant in this band, with the average vibrational spacing being 0.087 eV (0.101 eV in the ground-state). Additional assignments have been proposed from the fluorescence spectroscopy work of Okuyama et al. [16] and are due to C–C stretching, $\nu'_{19}(a')$, C–H in-plane bending, $\nu'_{20}(a')$ and C–F bending, $\nu'_{24}(a')$ and $\nu'_{25}(a')$ modes. A close inspection of Fig. 3 also shows shoulder structures on the low energy onset to the band, some of them tentatively assigned to hot-bands (Table 2) and also being part of the unresolved internal rotational contribution of the methyl group. The feature at 4.56(7) eV remains unassigned, but may be either a hot-band of the C–CH_3 stretching mode $\nu'_{23}(a')$ or a branch member of the rotational envelope.

The geometry of 2-fluorotoluene in the first excited state together with its bond lengths in Å and bond angles in (°), obtained

Table 3
Proposed vibrational assignments in the 5.9–6.9 eV absorption band of 2-fluorotoluene, 2-C_7H_7F.

Energy (eV)	Assignment	ΔE (eV)
5.92(4)(s)	0_0^0	–
6.01(9)(b)	21_0^1	0.095
6.129	$3p(5a'')^{-1}/3s(4a'')^{-1}$	–
6.21(5)(b,w)	21_0^1	0.086
6.30(6)(b,w)	21_0^2	0.091
6.77(9)(s,w)	0_0^0	–
6.81(8)(s)	25_0^1	0.039
6.858	$25_0^2/3p'(5a'')^{-1}/3p(4a'')^{-1}$	0.040

(s) shoulder feature; (b) broad structure; (w) weak structure (the last decimal of the energy value is given in brackets for these less-resolved features)

at the TD-DFT/CAMB3LYP/aug-cc-pVDZ level of theory are shown in Fig. S3. The role of the first excited state, denoted in the literature as S_1, in the electronic state spectroscopy of 2-C_7H_7F has been investigated due to the methyl group internal rotation and the mechanism related to the interaction between the ring π^* MO and the methyl CH σ^* orbital in the LUMO. This interaction has been termed as π^*–σ^* hyperconjugation [16], i.e., if it occurs in the S_1 state, the methyl CH bonds strengths are reduced by the partial electron transfer process that can occur from the π^* MO to the σ^* antibonding orbital [4]. We observe from the calculated bond lengths that while C11–H14 is slightly elongated from the neutral ground-state (S_0), the other C–H bonds (C11–H12 and C11–H13) do not change appreciably. However, H14 in the S_1 state points out-of-plane which can symmetry favour an intramolecular electron transfer from the ring to its σ^* antibonding orbital, while the other methyl C–H bonds remain almost within the ring plane thus lending strong support to spatially prohibited hyperconjugation [4]. This in turn means a considerable coupling between the methyl group internal rotation and C–H stretching vibration, where the most active mode in the lowest-lying absorption band, C–F/C–H stretching $\nu'_{21}(a')$, is reduced by ~ 15% from its value in the electronic ground-state (Tables S3 and S4).

5.1.2. Valence and vibronic excitation in the range 5.5–10.8 eV

Centred at 6.129 eV with a maximum cross-section of 24.68 Mb, the second absorption band is assigned mainly due to the Rydberg $3s(25a') \leftarrow \pi(5a'')(1^1A'' \leftarrow \tilde{X}^1A')$ transition with an $f_L \approx 0.0066$, although with a similar order of magnitude oscillator strength ($f_L \approx 0.0051$) it can also be ascribed to the $\pi^*(8a'') \leftarrow \pi(5a'') + \pi^*(7a'') \leftarrow \pi(4a'')(3^1A' \leftarrow \tilde{X}^1A')$ transition (Table S1). However, at the TD-DFT/CAMB3LYP/aug-cc-pvDZ level of calculation (see Table 1), the feature is mainly assigned to a valence $\pi^*(7a'') \leftarrow \pi(5a'') + \pi^*(6a'') \leftarrow \pi(4a'')(3^1A' \leftarrow \tilde{X}^1A')$ transition ($f_L \approx 0.0082$), yet a mixed valence-Rydberg contribution $3p/\pi^*(25a') \leftarrow \pi(5a'')(1^1A'' \leftarrow \tilde{X}^1A')$ with $f_L \approx 0.0073$ is also possible. Looking at the absorption band in Fig. 4, the rather broad nature of the features may be indicative of a more valence character. Notwithstanding, the less pronounced features compared to the lowest-lying band are listed and assigned in Table 3. For the valence excitation the main vibrational modes are due to a few quanta of C–F/C–H stretching, $\nu'_{21}(a')$ and C–F bending, $\nu'_{25}(a')$ modes.

The most intense absorption band in the VUV spectrum of 2-fluorotoluene with a maximum at 6.858 eV and a cross-section of 212.39 Mb (Figs. 2 and 5) is assigned to a $\pi^*(7a'') \leftarrow \pi(4a'') + \pi^*(6a'') \leftarrow \pi(5a'')(5^1A' \leftarrow \tilde{X}^1A')$ transition from the TD-DFT/CAMB3LYP/aug-cc-pvDZ calculation in Table 1 with $f_L \approx 0.6859$. We note that at the EOM-CCSD/aug-cc-pVDZ level of theory (see Table S1), such an electronic transition may also contain Rydberg character (see Section 5.2). The 0_0^0 origin band is assigned at 6.77(9) eV (Table 3) and shows two quanta of the C–F bending, $\nu'_{25}(a')$ mode. The next valence transition peaking at 9.454 eV has its 0_0^0 origin band at 9.253 eV and is accompanied by six quanta of C–CH_3 stretching mode $\nu'_{23}(a')$, with mean energy value of 0.069 eV (Table 4 and Fig. 7). The next band peaking at 10.039 eV, and according to the calculations in Table 1, has been assigned to the $3d(29a') \leftarrow \sigma_{CC}/\tilde{n}_F(24a')(25^1A' \leftarrow \tilde{X}^1A')$ Rydberg transition (see Section 5.2 and Table 5). It has a reasonably high oscillator strength (≈ 0.0422) and contributes to the feature observed in this energy range. The 0_0^0 transition at 9.770 eV (Table 4) can also be related to the mixed valence-Rydberg transition calculated at 10.113 eV (see Table S2) with $f_L \approx 0.0409$, and assigned to the contribution of HOMO-3 to LUMO+2 (30%) $3s(26a') \leftarrow \pi/n_F(3a'')$, HOMO-1 to LUMO+19 (15%) $\sigma^*_{CH}/\pi^*(38a') \leftarrow \pi(4a'')$ and HOMO-1 to LUMO+22 (21%) $\pi^*(40a') \leftarrow \pi(4a'')$. Several quanta of C–$CH_3$ stretching mode $\nu'_{23}(a')$, with mean energy value of 0.066 eV, are excited.

5.2. Rydberg transitions

The photoabsorption spectrum displays several features above 6.1 eV relating to the different Rydberg states converging to the lowest-lying ionisation energies (IEs). The experimental adiabatic ionisation energy value (IE_1) of Watanabe *et al.* [27] is used to estimate the Rydberg series converging to the $(5a'')^{-1}$ $\tilde{X}^2A''$ ionic electronic ground-state, whereas the experimental vertical ionisation energies of IE_2, IE_3, IE_4 and IE_5, $(4a'')^{-1}$ $\tilde{A}^2A''$, $(24a')^{-1}$ $\tilde{B}^2A'$, $(23a')^{-1}$ $\tilde{C}^2A''$ and $(3a'')^{-1}$ $\tilde{D}^2A''$ ionic electronic excited states, respectively, are obtained from Palmer and co-workers [26]. The proposed Rydberg structures are labelled in Figs. 4–7 and listed in Table 5.

The peak positions have been tested using the Rydberg formula: $E_n = E_i - R / (n - \delta)^2$, where E_i is the ionisation energy, n is the principal quantum number of the Rydberg orbital of energy E_n, R is the Rydberg constant (13.61 eV), and δ the quantum defect resulting from the penetration of the Rydberg orbital into the core. As far as the authors are aware, although some of the Rydberg features of 2-fluorotoluene have been reported before [23], the present assignments correspond to the most complete analysis of such states. Some of these Rydberg progressions overlap with each other and most display vibrational structure in addition to the main spectral features (Tables 3 and 4). These contributions tend to broaden the absorption peaks.

The lowest-lying member of the $(ns \leftarrow 5a'')$ Rydberg transition is not discernible from the absorption spectrum. The 7.47(6) eV feature is tentatively assigned to 4s Rydberg series converging to the ionic electronic ground state, with a quantum defect $\delta = 0.93$ (Table 5), although it can also be assigned to a $3p'(4a'')^{-1}$ Rydberg transition. It is accompanied by one quantum of the C–CH_3 stretching mode $\nu'_{23}(a')$, with a value of 0.060 eV (Figs. 4 and Table 4). Assignments for higher members are proposed in Table 5 up to $n = 9$, while features at 8.628 eV ($n = 8s$) and 8.696 eV ($n = 9s$), have also been assigned to $7d'(5a'')^{-1}/7d(4a'')^{-1}$ and $8d'(5a'')^{-1}$ Rydberg members, respectively. The first members of the np, np' and nd series are associated with the peaks at 6.129 eV ($\delta = 0.79$), 6.856 eV ($\delta = 0.43$) and 7.27(8) eV ($\delta = 0.12$), respectively, with the 6.129 eV feature also assigned to $3s(4a'')^{-1}$ (Table 5). The nd' series does not exhibit the $n = 3$ feature, so its first member assigned to 4d' is visible at 8.033 eV (it can also be assigned to $4s(4a'')^{-1}$) with a quantum defect $\delta = 0.07$ (Table 5) and extends up to $n = 8$. Features at 6.856, 8.463, 8.60(4), 8.66(1) and 8.716 eV are also due to Rydberg transitions to $3p(4a'')^{-1}$, $4p'(4a'')^{-1}$, $4d(4a'')^{-1}$, $4d'(4a'')^{-1}$ and $5s(4a'')^{-1}$, respectively (Table 5). Vibrational excitation involving some of the members of these Rydberg series has been assigned to the C–CH_3 stretching mode $\nu'_{23}(a')$, in

Table 4
Proposed vibrational assignments in the 7.4–10.3 eV absorption band of 2-fluorotoluene, 2-C_7H_7F.

Energy (eV)	Assignment	ΔE (eV)	Energy (eV)	Assignment	ΔE (eV)	Energy (eV)	Assignment	ΔE (eV)
7.47(6)(s)	$4s(5a'')^{-1}/3p'(4a'')^{-1}$	–	8.16(0)(w)	$5p(5a'')^{-1}$	–	9.253	$0_0^0/8s(4a'')^{-1}$	–
7.53(9)(s,b)	$4p(5a'')^{-1}/23_0^1$	0.060	8.230	23_0^1	0.070	9.32(2)(b)	$23_0^1/3s(23a')^{-1}$	0.069
			8.302	23_0^2	0.072	9.39(6)(s)	23_0^2	0.074
7.64(4)(s,b)	23^n	–				9.454	23_0^3	0.058
7.71(1)(b,w)	23^{n+1}	0.067	8.302	$4p(4a'')^{-1}$	–	9.52(3)(b)	23_0^4	0.069
7.773	23^{n+2}	0.062	8.363	23_0^1	0.061	9.58(9)(b,w)	23_0^5	0.066
7.842	23^{n+3}	0.069	8.43(1)(b)	23_0^2	0.068	9.66(4)(b,w)	23_0^6	0.075
			8.49(8)(s)	$23_0^2/6d(5a'')^{-1}$	0.067			
7.79(8)(s)	$3d(4a'')^{-1}$	–				9.770	0_0^0	–
7.86(0)(s)	23_0^1	0.062	8.39(2)(w)	$6s(5a'')^{-1}$	–	9.840	23_0^1	0.070
7.933	$23_0^2/3d'(4a'')^{-1}$	0.073	8.463	$23_0^1/6p'(5a'')^{-1}/4p'(4a'')^{-1}$	0.071	9.90(7)(s)	23_0^2	0.067
						9.975	$23_0^3/3p(23a')^{-1}$	0.068
7.89(2)(b)	$4p'(5a'')^{-1}$	–	8.463	$6p'(5a'')^{-1}/4p'(4a'')^{-1}$	–	10.039	$23_0^4/3p'(24a')^{-1}$	0.064
7.968	23_0^1	0.076	8.530	$23_0^1/6d'(5a'')^{-1}$	0.067	10.10(5)(b,w)	23_0^5	0.066
8.033	$23_0^2/4s(4a'')^{-1}$	0.065	8.60(4)(b)	$23_0^2/7p'(5a'')^{-1}/4d(4a'')^{-1}$	0.074	10.175	23_0^6	0.070
8.101	$23_0^3/4s(5a'')^{-1}$	0.068	8.67(9)(s)	$23_0^3/8p'(5a'')^{-1}$	0.075	10.234	23_0^7	0.059
			8.741	$23_0^4/9d(5a'')^{-1}$	0.062			
7.933	$3d'(4a'')^{-1}$	–						
8.00(2)(s)	$23_0^1/4d(5a'')^{-1}/4d'(5a'')^{-1}$	0.069	8.49(8)(s)	$6d(5a'')^{-1}$	–			
8.064	23_0^2	0.062	8.56(0)(s)	$23_0^1/7p(5a'')^{-1}$	0.062			
8.133	23_0^3	0.069	8.628	$23_0^2/7d'(5a'')^{-1}$	0.068			
			8.698	$23_0^3/9s(5a'')^{-1}/8d'(5a'')^{-1}$	0.070			
			8.775	$23_0^4/5p(4a'')^{-1}$	0.077			
			8.84(3)(s)	23_0^5	0.068			
			8.913	23_0^6	0.070			

s) shoulder structure; (w) weak structure; (b) broad structure (the last decimal of the energy value is given in brackets for these less-resolved features).

Table 5
Energy values (eV), quantum defects (δ) and assignments of the Rydberg series converging to $(5a'')^{-1}$ $\tilde{X}^2A''$, $(4a'')^{-1}$ $\tilde{A}^2A''$, $(24a')^{-1}$ $\tilde{B}^2A'$, $(23a')^{-1}$ $\tilde{C}^2A''$ and $(3a'')^{-1}$ $\tilde{D}^2A''$ ionic states of 2-fluorotoluene, 2-C_7H_7F.

E_n	δ	Assignment	E_n	δ	Assignment	E_n	δ	Assignment
$(IE_1)_{ad}$ = 8.915 eV $(5a'')^{-1}$			**$(IE_1)_{ad}$ = 8.915 eV** $(5a'')^{-1}$			**$(IE_2)_v$ = 9.53 eV** $(4a'')^{-1}$		
(ns ← 5a'')			*(nd' ← 5a'')*			*(nd' ← 4a'')*		
–	–	3s	–	–	3d'	7.933	0.08	3d'
7.47(6)(b,w)	0.93	4s	8.033	0.07	4d'	8.66(1)(s,w)	0.04	4d'
8.101	0.91	5s	8.35(8)(s)	0.06	5d'	8.98(4)(b,w)	0.01	5d'
8.39(2)(w)	0.90	6s	8.530	0.05	6d'	**$(IE_3)_v$ = 12.08 eV** $(24a')^{-1}$		
8.54(5)(s,w)	0.94	7s	8.628	0.11	7d'	*(ns ← 24a')*		
8.628	1.11	8s	8.698	0.08	8d'	8.695	0.99	3s
8.698	1.08	9s	**$(IE_2)_v$ = 9.53 eV** $(4a'')^{-1}$			10.57(9)(s,w)	0.99	4s
(np ← 5a'')			*(ns ← 4a'')*			*(np ← 24a')*		
6.129	0.79	3p	6.129	1.00	3s	9.32(2)(b)	0.78	3p
7.53(9)(s,b)	0.86	4p	8.033	0.99	4s	10.76(7)(s)	0.78	4p
8.16(0)(w)	0.75	5p	8.716	0.91	5s	*(np' ← 24a')*		
8.42(0)(w)	0.76	6p	8.99(1)(b,w)	0.98	6s	10.039	0.42	3p'
8.56(0)(s)	0.81	7p	9.15(4)(b,w)	0.98	7s	*(nd ← 24a')*		
8.66(1)(s,w)	0.68	8p	9.253	0.99	8s	10.32(3)(w)	0.22	3d
8.716	0.73	9p	9.32(2)(b)	0.91	9s	*(nd' ← 24a')*		
(np' ← 5a'')			*(np ← 4a'')*			10.49(8)(w)	0.07	3d'
6.856	0.43	3p'	6.856	0.74	3p	**$(IE_4)_v$ = 12.65 eV** $(23a')^{-1}$		
7.89(2)(b)	0.35	4p'	8.302	0.67	4p	*(ns ← 23a')*		
8.26(3)(s)	0.43	5p'	8.775	0.75	5p	9.32(2)(b)	0.98	3s
8.463	0.51	6p'	9.03(4)(s,b)	0.76	6p	*(np ← 23a')*		
8.60(4)(b)	0.39	7p'	9.18(1)(s,w)	0.75	7p	9.983	0.74	3p
8.67(9)(s)	0.41	8p'	*(np' ← 4a'')*			*(np' ← 23a')*		
(nd ← 5a'')			7.47(6)(b,w)	0.43	3p'	10.61(1)(s,w)	0.42	3p'
7.27(8)(s,w)	0.12	3d	8.463	0.43	4p'	**$(IE_5)_v$ = 14.00 eV** $(3a'')^{-1}$		
8.00(2)(s)	0.14	4d	8.875	0.44	5p'	*(ns ← 3a'')*		
8.33(8)(s)	0.14	5d	9.09(0)(b)	0.44	6p'	10.61(1)(s)	1.00	3s
8.49(8)(s)	0.29	6d	*(nd ← 4a'')*					
8.628	0.11	7d	7.79(8)(s)	0.20	3d			
–	–	8d	8.60(4)(b)	0.17	4d			
8.741	0.16	9d	8.93(6)(b,w)	0.21	5d			
			9.12(3)(b,w)	0.22	6d			

(w) weak structure; (b) broad feature; (s) shoulder structure (the last decimal on the energy value is given in brackets for these less-resolved features).

Table 4. The higher members of the series, for which the relative intensity decreases, are difficult to assign due to overlap with other transitions and possible vibronic structure (Table 4).

Following a similar methodology as for the valence transitions, the geometry of 2-C_7H_7F in the cationic ground state together with its bond lengths in Å and bond angles in (°), has also been obtained at the DFT/CAMB3LYP/aug-cc-pVDZ level of theory and is depicted in Fig. S4. A close comparison of the normal mode description shows that C–F bending $\nu'_{25}(a')$, is reduced by 12% from its value in the electronic ground-state (Tables S3 and S4), which is in favour of the increased C2 – F15 bond length. Note also that in the cation the bond angle $\measuredangle$ C1–C2–F15 is 116.44° against 117.88° in the ground-state, which may provide a weakening of the C – F bond strength. This agrees with the proposed assignment in Table 3 for the lowest-lying members of the Rydberg series. Another aspect pertains to C – C in plane bending $\nu'_{23}(a')$ mode, which is not significantly affected from its value in the ground state (less than 1%), thus lending support to the assignment in Table 4.

The first members of the *n*s, *n*p, *n*p', *n*d and *n*d' series converging to the ionic electronic first excited state of 2-fluorotoluene $(4a'')^{-1}$ are associated with the peaks at 6.129 eV ($\delta = 1.00$), 6.856 eV ($\delta = 0.74$), 7.47(6) eV ($\delta = 0.43$), 7.79(8) eV ($\delta = 0.20$) and 7.993 eV ($\delta = 0.08$), respectively (Table 5). The feature at 9.32(2) eV can also be assigned to $3p(24a')^{-1}$ and $3s(23a')^{-1}$. Rydberg transitions (Figs. 4–7) are accompanied by vibronic structure which is due to excitation of C–CH_3 stretching mode $\nu'_{23}(a')$, (Table 4).

The Rydberg series converging to the ionic electronic second excited state, $n = 3$ for *n*s, *n*p, *n*p', *n*d and *n*d' are proposed at 8.695, 9.32(2), 10.039, 10.32(3) and 10.49(8) eV, respectively, (Table 5) with quantum defects 0.99, 0.78, 0.42, 0.22 and 0.07, respectively. Note that the quantum defect obtained for the 10.039 eV feature is indicative of a *n*p member, whereas the calculations in Table 2 predict a 3d Rydberg character. Some of the fine structure has been assigned to vibrational excitation involving C–CH_3 stretching mode $\nu'_{23}(a')$ (see Table 4).

Finally, the features at 9.32(2), 9.983 and 10.61(1) eV are assigned to $3s(23a')^{-1}$ ($\delta = 0.98$), $3p(23a')^{-1}$ ($\delta = 0.74$) and $3p'(23a')^{-1}$ ($\delta = 0.42$) members of Rydberg series converging to the ionic electronic third excited state, while at 10.61(1) eV to $3s(3a'')^{-1}$ with a quantum defect $\delta = 1.00$. We have not made any attempt to identify higher members of the Rydberg series, either due to the broad and structureless nature of the absorption bands or just simply because they lay outside the energy range of the present photoabsorption spectrum.

5.3. Absolute photoabsorption cross sections and atmospheric photolysis

The absolute photoabsorption cross-section values for the major electronic transitions are listed in Tables 1 and S1 (in units of Mb). A thorough literature survey reveals a lack of any former absolute absorption studies to compare with the present data in the photon energy region 4.4–10.8 eV. The present absolute cross-sections below 6.89 eV (above 180 nm) can be used in combination with solar actinic flux measurements from the literature [44] to estimate the photolysis rate of 2-fluorotoluene in the atmosphere from an altitude close to the ground to the stratopause at 50 km. Details of the calculation programme can be found elsewhere [45] in which the quantum yield for dissociation following absorption is assumed to be unity. The reciprocal of the photolysis rate at a given altitude corresponds to the local photolysis lifetime.

Photolysis lifetimes of less than 5 sunlit days were calculated at altitudes above 20 km with less than a day above 24 km. We are not aware of any detailed investigation, neither on the rate coefficients obtained for reactions between the OH radical and 2-fluorotoluene, that may provide a main reactive sink mechanism in the troposphere, nor from secondary organic aerosol formation from the oxidation of 2-C_7H_7F by chlorine atoms. The latter is known to be as important as hydroxyl-radical-initiated oxidation in the early morning in certain coastal or industrialized areas, as reported for toluene [21]. Thus, until further relevant information within the international community, it stands to be proven which mechanism may prevail as the relevant sink of 2-fluorotoluene.

6. Conclusions

The present experimental and theoretical joint work provides the first complete study to date of the VUV electronic state spectroscopy of 2-fluorotoluene and provides the most reliable set of absolute photoabsorption cross sections between 4.4 to 10.8 eV. The main absorption features are due to electronic excitations from the ground state to valence, mixed valence-Rydberg and Rydberg states, with novel assignments in the photon energy covered in this work, which have not been previously reported in the literature. Theoretical calculations on the vertical excitation energies and oscillator strengths were performed using the equation-of-motion coupled cluster method restricted to the single and double excitations (EOM-CCSD) and time-dependent density functional theory (TD-DFT), the former more attuned to the lowest-lying electronic states, the latter giving a better agreement with the experimental findings above 7 eV. The analysis of the observed vibronic structure in the photoabsorption spectrum has been assigned to C–C stretching, $\nu'_{19}(a')$, C–H in-plane bending, $\nu'_{20}(a')$, C–F/C–H stretching, $\nu'_{21}(a')$, C–CH_3 stretching, $\nu'_{23}(a')$ and C–F bending, $\nu'_{24}(a')$ and $\nu'_{25}(a')$ modes. The photolysis lifetimes of 2-fluorotoluene have also been obtained for the Earth's troposphere and stratosphere.

Author statement

PASR and ASB have performed the quantum chemical calculations; ASB, MB and PLV wrote the manuscript draft; SK, AIL, NCJ, SVH have contributed with the experimental aspects of the synchrotron beam line used for the experiments; ASB, MB, NCJ, SVH and PLV revised the manuscript.

Declaration of Competing Interest

The authors declare that they have no known competing financial interests or personal relationships that could have appeared to influence the work reported in this paper.

Data availability

Data will be made available on request.

Acknowledgments

PASR acknowledges support from the Brazilian agency Coordenação de Aperfeiçoamento de Pessoal de Nível Superior (CAPES). ASB and MHFB acknowledge support from the Brazilian agency Conselho Nacional de Desenvolvimento Científico e Tecnológico (CNPq). PASR, ASB and MHFB also acknowledge Prof. Carlos de Carvalho for computational support at LFTC-DFis-UFPR and at LCPAD-UFPR. The authors wish to acknowledge the beam time at the ISA synchrotron, Aarhus University, Denmark. The research leading to this result has been supported by the project CALIPSOplus under the Grant Agreement 730872 from the EU Framework Programme for Research and Innovation HORIZON 2020. SK, AIL and PLV acknowledges the Portuguese National Funding Agency (FCT) through research grant CEFITEC (UIDB/00068/2020). PLV also acknowledges

his visiting professor position at Federal University of Paraná, Curitiba, Brazil. This contribution is also based upon work from the COST Action CA18212-Molecular Dynamics in the GAS phase (MD-GAS), supported by COST (European Cooperation in Science and Technology).

Supplementary materials

Supplementary material associated with this article can be found, in the online version, at doi:10.1016/j.jqsrt.2023.108597.

References

[1] Yang SK, Liu SY, Chen HF, Lee YP. Molecular elimination in photolysis of o- and p-fluorotoluene at 193 nm: Internal energy of HF determined with time-resolved Fourier transform spectroscopy. J Chem Phys 2005;123:224304.
[2] Timbers PJ, Parmenter CS, Moss DB. Acceleration of intramolecular vibrational redistribution by methyl internal rotation. II. A comparison of m-fluorotoluene and p-fluorotoluene. J Chem Phys 1994;100:1028–34.
[3] Davies AR, Kemp DJ, Wright TG. Methyl-torsion-facilitated internal energy delocalization following electronic excitation in m -fluorotoluene: Can meta and para substitution be directly compared? AIP Adv 2020;10:125206.
[4] Chiba T, Okuyama K, Fujii A. Observation of evidence for the π-$\sigma*$ hyperconjugation in the S1 State of o-, m-, and p-fluorotoluenes by double-resonance infrared spectroscopy. J Phys Chem A 2016;120:5573–80.
[5] Cvitas T, Hollas JM. A partial analysis of rotational structure in the 2710 Å system of p-fluorotoluene. Mol Phys 1971;20:645–54.
[6] Gardner AM, Whalley LE, Kemp DJ, Tuttle WD, Wright TG. Identification of separate isoenergetic routes for vibrational energy flow in p-fluorotoluene. J Chem Phys 2019;151:154302.
[7] Gardner AM, Tuttle WD, Whalley LE, Wright TG. Direct observation of vibrational energy dispersal: via methyl torsions. Chem Sci 2018;9:2270–83.
[8] Gascooke JR, Stewart LD, Sibley PG, Lawrance WD. Pervasive interactions between methyl torsion and low frequency vibrations in S0 and S1 p-fluorotoluene. J Chem Phys 2018;149:074301.
[9] Kemp DJ, Whalley LE, Gardner AM, Tuttle WD, Warner LG, Wright TG. Complexity surrounding an apparently simple Fermi resonance in p -fluorotoluene revealed using two-dimensional laser-induced fluorescence (2D-LIF) spectroscopy. J Chem Phys 2019;150:064306.
[10] Scott DW, Messerly JF, Todd SS, Hossenlopp IA, Douslin DR, McCullough JP. 4-fluorotoluene: chemical thermodynamic properties, vibrational assignment, and internal rotation. J Chem Phys 1962;37:867–73.
[11] Tuttle WD, Gardner AM, Whalley LE, Wright TG. Vibration and vibration-torsion levels of the S1 state of para -fluorotoluene in the 580-830 cm-1 range: interactions and coincidences. J Chem Phys 2017;146:244310.
[12] Gardner AM, Tuttle WD, Whalley L, Claydon A, Carter JH, Wright TG. Torsion and vibration-torsion levels of the S1 and ground cation electronic states of para -fluorotoluene. J Chem Phys 2016;145:124307.
[13] Susskind J. Microwave spectrum, barrier to internal rotation, and torsion-vibration interaction in ortho-fluoro toluene. J Chem Phys 1970;53:2492–501.
[14] Rottstegge J, Hartwig H, Dreizler H. The rotational spectrum, structure and barrier V6 to internal rotation of p-fluorotoluene. J Mol Struct 1999;478:37–47.
[15] Stewart LD, Gascooke JR, Lawrance WD. A strong interaction between torsion and vibration in S 0 and S 1 m -fluorotoluene. J Chem Phys 2019;150:174303.
[16] Okuyama K, Mikami N, Ito M. Internal rotation of the methyl group in the electronically excited state: o-, m-, and p-fluorotoluene. J Phys Chem 1985;89:5617–25.
[17] Nair KPR, Herbers S, Nguyen HVL, Grabow JU. The structure and low-barrier methyl torsion of 3-fluorotoluene. Spectrochim Acta, Part A 2020;242:118709.
[18] Jacobsen S, Andresen U, Mäder H. Microwave spectra of o-fluorotoluene and its 13C isotopic species: methyl internal rotation and molecular structure. Struct Chem 2003;14:217–25.
[19] Herbers S, Buschmann P, Wang J, Lengsfeld KG, Nair KPR, Grabow JU. Reactivity and rotational spectra: the old concept of substitution effects. Phys Chem Chem Phys 2020;22:11490–7.
[20] Davies AR, Kemp DJ, Wright TG. Unpicking vibration-vibration and vibration–torsion interactions in m-fluorotoluene. J Mol Spectrosc 2021;381:111522.
[21] Serralheiro C, Duflot D, Da Silva FF, Hoffmann SV, Jones NC, Mason NJ, et al. Toluene valence and Rydberg excitations as studied by ab initio calculations and vacuum ultraviolet (VUV) synchrotron radiation. J Phys Chem A 2015;119:9059–69.
[22] Barbosa AS, Da SFF, Rebelo A, Hoffmann SV, Bettega MHF, Limão-Vieira P. Valence and Rydberg excitations of 2,4- And 2,6-difluorotoluene as studied by vacuum ultraviolet synchrotron radiation and ab initio calculations. J Phys Chem A 2016;120:8998–9007.
[23] Hammond VJ, Price WC, Teegan JP, Walsh AD. The absorption spectra of some substituted benzenes and naphtalenes in the vacuum ultra-violet. Discuss Faraday Soc 1950;9:53–60.
[24] Cave WT, Thompson HW. The ultra-violet absorption spectra of fluorinated toluenes. Discuss Farad Soc 1950;9:35–46.
[25] Lias SG, Ausloss P. Ionization energies of organic compounds by equilibrium measurements. J Am Chem Soc 1978;100:6027–34.
[26] Palmer MH, Moyes W, Spiers M, Ridyard JNA. The electronic structure of substituted benzenes; Ab initio calculations and photoelectron spectra for the methyl- and fluoro-benzenes and fluorotoluenes. J Mol Struct 1978;49:105–23.
[27] Watanabe K, Nakayama T, Mottl J. Ionization potentials of some molecules. J Quant Spectrosc Radiat Transf 1962;2:369–82.
[28] Thompson BHW, Temple RB. Infra-red spectra of fluorinated hydrocarbons. Part III. J Chem Soc 1948:1432–6.
[29] Joshi G, Singh NL. absorption spectrum of ortho-fluorotoluene. Spectrochim Acta 1967;23:1341–4.
[30] Green JHS. Vibrational spectra of benzene derivatives-IX. o-Disubstituted compounds. Spectrochim Acta, Part A 1970;26:1913–23.
[31] Suryanarayana V, Rao IA, Rao VR. The fluorescence and emission spectra of the three isomeric fluoro-toluenes. Trans Faraday Soc 1957;53:1570–7.
[32] Koto E, Furuya K, Ogawa T. Direct observation of intramolecular vibrational energy redistribution under white light excitation. II. Fluorescence spectra of fluorobenzene derivatives by controlled electron impact. Spectrochim Acta, Part A 2000;56:515–21.
[33] Emrich K. An extension of the coupled cluster formalism to excited states (I). Nucl Phys 1981;;A351:379–96.
[34] Sekino H, Bartlett RJ. A linear response, coupled-cluster theory for excitation energy. Int J Quantum Chem 1984;26:255–65.
[35] Stanton JF, Bartlett RJ. The equation of motion coupled-cluster method. A systematic biorthogonal approach to molecular excitation energies, transition probabilities, and excited state properties. J Chem Phys 1993;98:7029–39.
[36] Bartlett RJ. Coupled-cluster theory and its equation-of-motion extensions. Wiley Interdiscip Rev Comput Mol Sci 2012;2:126–38.
[37] Bauernschmitt R, Ahlrichs R. Treatment of electronic excitations within the adiabatic approximation of time dependent density functional theory. Chem Phys Lett 1996;256:454–64.
[38] Casida ME. Time-dependent density-functional theory for molecules and molecular solids. J Mol Struct-Theochem 2009;914:3–18.
[39] Yanai T, Tew DP, Handy NC. A new hybrid exchange-correlation functional using the Coulomb-attenuating method (CAM-B3LYP). Chem Phys Lett 2004;393:51–7.
[40] Barca GMJ, Bertoni C, Carrington L, Datta D, De Silva N, Deustua JE, et al. Recent developments in the general atomic and molecular electronic structure system. J Chem Phys 2020;152:154102.
[41] Parrish RM, Burns LA, Smith DGA, Simmonett AC, DePrince AE, Hohenstein EG, et al. Psi4 1.1: an open-source electronic structure program emphasizing automation, advanced libraries, and interoperability. J Chem Theory Comput 2017;13:3185–97.
[42] Palmer MH, Ridley T, Hoffmann SV, Jones NC, Coreno M, De Simone M, et al. Interpretation of the vacuum ultraviolet photoabsorption spectrum of iodobenzene by ab initio computations. J Chem Phys 2015;142:134302.
[43] Eden S, Limão-Vieira P, Hoffmann SV, Mason NJ. VUV photoabsorption in CF3X (X = Cl, Br, I) fluoro-alkanes. Chem Phys 2006;323:313–33.
[44] . Chemical kinetics and photochemical data for use in stratospheric modelling, evaluation number 12, 97-4. NASA, Jet Propulsion Laboratory, JPL, Publication; 1997.
[45] Limão-Vieira P, Eden S, Kendall PA, Mason NJ, Hoffmann SVV. Photo-absorption cross-section for CCl2F2. Chem Phys Lett 2002;364:535–41.